ELSEVIER

Journal of Power Sources 68 (1997) 698–703

JOURNAL OF POWER SOURCES

The amorphous oxides $MnV_2O_{6+\delta}$ $(0<\delta<1)$ as high capacity negative electrode materials for lithium batteries

Y. Piffard, F. Leroux *, D. Guyomard, J.-L. Mansot, M. Tournoux

Laboratoire de Chimie des Solides, Institut des Matériaux de Nantes, UMR CNRS No 110, 2 rue de la Houssinière, 44072 Nantes Cedex 03, France

Accepted 21 September 1996

Abstract

$MnV_2O_{6+\delta}\cdot nH_2O$ $(0<\delta<1)$ amorphous oxides were prepared by a two-step process including the precipitation of a crystallized precursor $MnV_2O_6\cdot 4H_2O$ and its ozonation at temperatures below 100 °C. Their characterization by spectroscopic techniques (XAS and EELS) shows that V^{5+} retains a VO_5 environment and that Mn, which remains in octahedral coordination, is oxidized to Mn^{4+} mainly. $MnV_2O_{6+\delta}$ compounds insert reversibly large amounts of Li per formula unit (e.g. $Li_{12}MnV_2O_{6.96}$) at low voltage. After the first insertion/de-insertion cycle, subsequent cycles correspond to fully reversible lithium insertion between the two compositions: $Li_\alpha MnV_2O_{6+\delta}$ $(\alpha\geq 2)$ and $Li_{12}MnV_2O_{6+\delta}$ (from 600 to 900 mAh/g). Investigations on the Li derivatives by XAS and EELS show that during the insertion/de-insertion cycles the V oxidation state varies reversibly between +5 and +3. Mn^{4+} cations are reduced to Mn^{2+} upon the first discharge. During the subsequent cycles the average Mn oxidation state varies reversibly between +2 and about +2.6. It clearly appears that the electron transfer from Li to the host matrix decreases with increasing x in $Li_xMnV_2O_{6+\delta}$.

Keywords Lithium batteries; Negative electrodes, Manganese oxides, Vanadium oxides

1. Introduction

Among cathode materials, manganese and vanadium oxides have been, and are still intensively studied. With the aim of obtaining new cathode materials, investigations in the Mn–V–O system have been undertaken under different oxidizing conditions. Amorphous materials with quite an unexpected electrochemical behavior have been obtained. This paper first reports on their synthesis and characterization. Then, their electrochemical behavior with respect to lithium insertion is described along with a characterization of the lithiated derivatives, mainly by local techniques.

2. Experimental

2.1. Synthesis

$MnV_2O_{6+\delta}\cdot nH_2O$ $(0<\delta<1)$ amorphous mixed oxides were prepared by a two-step process including the preparation of a crystallized precursor $MnV_2O_6\cdot 4H_2O$ [1] and its ozonation at temperatures below 100 °C.

$MnV_2O_6\cdot 4H_2O$ was prepared as already mentioned in Ref. [2], by precipitation from a mixture of aqueous solutions of $NaVO_3$ $(2\times 10^{-2}$ M) and manganese nitrate, $Mn(NO_3)_2\cdot 4H_2O$ $(10^{-2}$ M) (equal volumes) at room temperature. This crystallized precursor was placed in a tubular furnace through which an O_2/O_3 mixture containing about 5% O_3 was flowing. It was heated in that manner for about 36 h, leading to $MnV_2O_{6+\delta}\cdot nH_2O$ amorphous products.

2.2. Characterization

A combination of thermal gravimetric analysis (TGA) and several spectroscopic techniques (XANES, EXAFS and EELS) was used to characterize the amorphous materials and their lithium derivatives.

2.3. Electrochemistry

Composite electrodes were prepared by mixing the active material, a carbon black (Super-S from Chemetals, Baltimore, MD, USA) and a binder (polyvinylidene difluoride

* Present address: Department of chemistry, University of Waterloo, 200 University Ave W., Waterloo, Ontario N2L 3G1, Canada

0378-7753/97/$17.00
PII S0378-7753(96)02576-1

(PVDF)) (85:10:5 mass ratio) and coating the mixture onto a stainless-steel disk serving as the current collector.

Standard laboratory swagelok test cells were used with the composite electrode as the positive and lithium metal as the negative, separated with glass paper soaked in the electrolyte. The electrolyte was made of 1 M $LiClO_4$ dissolved in a 2:1 mixture of ethylene carbonate (EC) and dimethyl carbonate (DMC). The cells were tested using the Mac-Pile system operating in a galvanostatic mode.

3. Characterization of $MnV_2O_{6+\delta}\cdot nH_2O$ compounds

3.1. Thermal behavior

The thermogravimetic (TG) curve of the material prepared at 95 °C is similar to that of the other members (Fig. 1). It shows two distinct weight loss processes:

(i) the first occurs between room temperature and 300 °C, it is reversible and could correspond to a water loss, and

(ii) the second, observed between 320 and 500 °C, is irreversible; it leads to the brannerite compound MnV_2O_6 and would correspond to an oxygen loss.

Accordingly, the formulae $MnV_2O_{6+\delta}\cdot nH_2O$ (Table 1) can be proposed for the amorphous materials. They show that as the ozonation temperature increases, the hydration rate decreases whereas the average oxidation state of Mn increases (we assume here that V retains its original oxidation state (+5) as this will be shown by spectroscopic measurements).

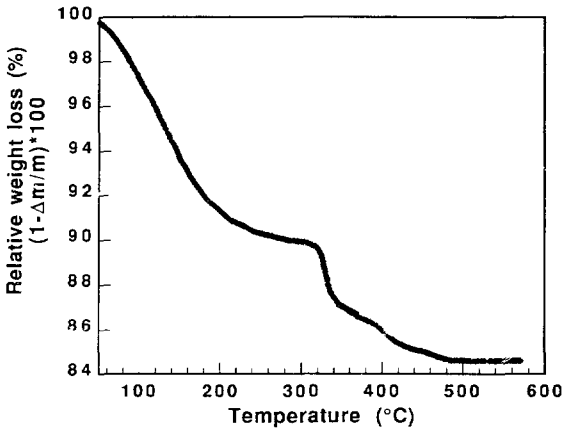

Fig. 1. Thermogravimetric curve of $MnV_2O_{6+\delta}\cdot nH_2O$ prepared at 95 °C.

Table 1
$MnV_2O6+\delta\cdot nH_2O$ chemical formulae inferred from TGA and average oxidation state of Mn inferred from TGA and EELS

Ozonation temperature (°C)	Chemical formula	Oxidation state of Mn from	
		TGA	EELS (I_3/I_2 intensity ratio)
25	$MnV_2O_{6.58}\cdot 3.4H_2O$	3.16	3.1±0.2
35	$MnV_2O_{6.81}\cdot 2.5H_2O$	3.62	3.4±0.2
65	$MnV_2O_{6.90}\cdot 2.1H_2O$	3.80	3.6±0.2
95	$MnV_2O_{6.96}\cdot 1.7H_2O$	3.92	4.0±0.2

3.2. Spectroscopic analyses

3.2.1. Extended X-ray absorption fine spectroscopy

The radial distribution function (RDF) of $MnV_2O_{6.96}$ (dehydrated), with V as a central atom, shows three distinct V–O peaks. Their refinement leads to three V–O distances very close to those encountered in the precursor $MnV_2O_6\cdot 4H_2O$ and a number of neighbors close to 5 (see results of the fits in the k space summarized in Table 2). Therefore, it appears that the ozonation does not change the arrangment of the first shell around the V atoms.

When Mn is the central atom, a comparison of the RDFs of $MnV_2O_{6.96}$ (dehydrated) and $MnV_2O_6\cdot 4H_2O$ shows a shift of the Mn–O peak for $MnV_2O_{6.96}$ toward shorter Mn–O distances. The refinement leads to an Mn–O distance of 1.89 Å in fair agreement with Mn^{4+} in a sixfold coordination, even though the number of neighbors refined is only 5.2 (Table 2). On account of the errors in the determination of this number and, as it will be shown below by the intensity of the pre-edge peak of the XANES spectrum, the expected number of neighbors, i.e. 6, is not in doubt.

3.2.2. XANES

The vanadium k-edge XANES spectra of $MnV_2O_{6.96}$ (dehydrated) and of $MnV_2O_6\cdot 4H_2O$ are displayed in Fig. 2. They are almost identical. An intense pre-edge peak is observed for both compounds. It corresponds to an electron transition from the core level (1s) to the p-symmetry part of the first non-completely filled energy level (molecular orbital mainly V(3d) type in the case of the vanadium k-edge). As a consequence, its intensity is indicative of a non-centrosymmetric environment of V atoms.

The Mn k-edge pre-edge spectra of MnO, Mn_2O_3, MnO_2 (IBA No. 15) and $MnV_2O_{6.96}$ are represented in Fig. 3. For all compounds the weak intensity of the pre-edge peak indicates that Mn occupies a symmetrical site. Furthermore, as the edge-jumps for MnO_2 (IBA No. 15) and $MnV_2O_{6.96}$ are

Table 2
Results of the fits for the first V and Mn coordination shells in $MnV_2O_{6.96}$ (inferred from EXAFS experiments) [a]

	d (Å)	N	σ (Å)	ΔE (eV)	ρ (%)
V–O	1.65	2.0			
	1.90	1.8	0.05	8.2	5
	2.06	1.0			
Mn–O	1.89	5.2	0.07	4.9	2

[a] N is the number of oxygen atoms surrounding the absorbing atom (V or Mn), σ is the Debye–Waller factor, ΔE and ρ represent the edge variation and the reliability factor of the fit, respectively

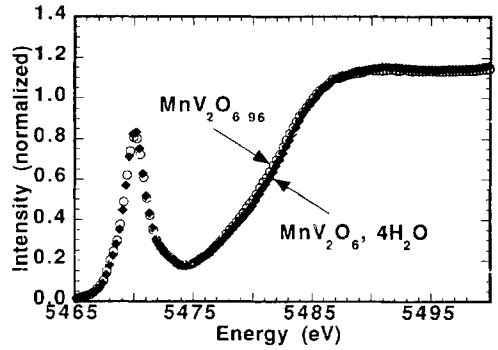

Fig. 2. Normalized V *k*-edge XANES spectra of $MnV_2O_6 \cdot 4H_2O$ and $MnV_2O_{6.96}$.

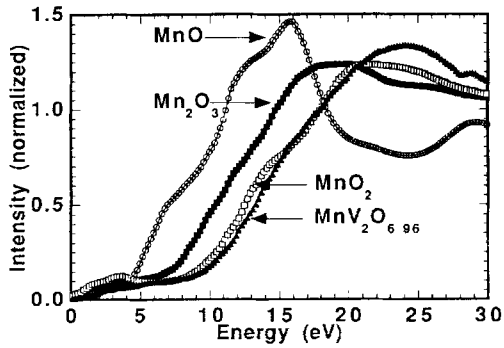

Fig. 3. Normalized Mn *k*-edge XANES spectra of MnO, Mn_2O_3, MnO_2 and $MnV_2O_{6.96}$.

very close to each other, the presence of Mn^{4+} in octahedral coordination is very likely in this latter compound.

3.2.3. *Electron energy loss spectroscopy*

The energy positions and intensities of the V and Mn $l_{2,3}$ peaks in $MnV_2O_6 \cdot 4H_2O$, MnV_2O_6 and the various $MnV_2O_{6+\delta} \cdot nH_2O$ materials were compared. As expected the V *l*-edge spectra are virtually the same in all compounds whereas a slight shift of the Mn *l*-edges toward higher energies is observed when the ozonation temperature increases. Accordingly, the white line l_3/l_2 intensity ratio decreases thus confirming an increase of the Mn oxidation state.

From the evolution of the white line l_3/l_2 intensity ratio as a function of the oxidation state of Mn in MnO, Mn_2O_3 and MnO_2 [3] average oxidation states can be proposed for Mn in $MnV_2O_{6+\delta} \cdot nH_2O$ materials (Table 1). They are in fair agreement with those inferred from TG experiments.

4. Electrochemical behavior

As $MnV_2O_{6+\delta} \cdot nH_2O$ materials can be dehydrated without changing the oxidation state of the transition metal cations, all the electrochemical experiments were carried out on dehydrated materials.

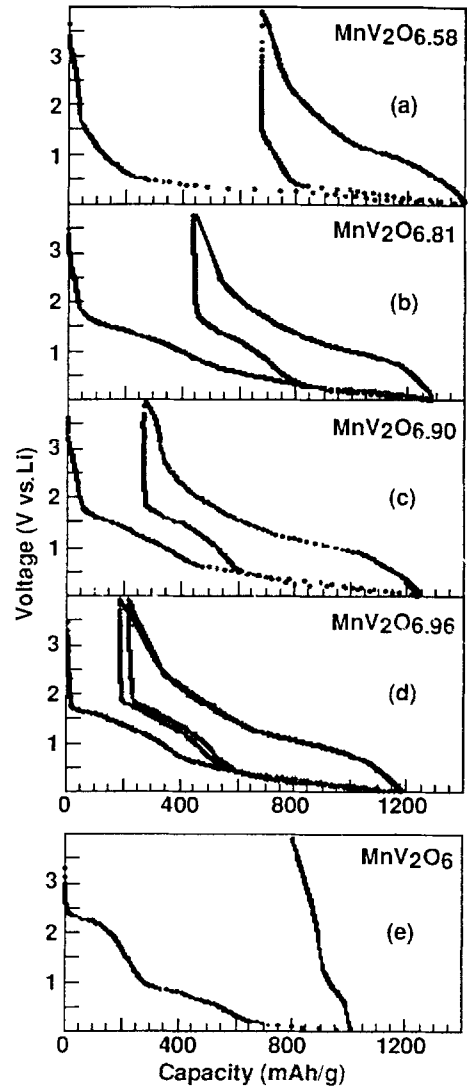

Fig. 4. Voltage–capacity curves for composite electrodes ($MnV_2O_{6+\delta}$ or (MnV_2O_6+C) (10 wt.%). (a) δ=0.58; (b) δ=0.81; (c) δ=0.90; (d) δ=0.96, and (e) MnV_2O_6.

Lithium insertion in $MnV_2O_{6+\delta}$ compounds was investigated under galvanostatic conditions (*C*/20 rate); typical chronopotentiometric curves are shown in Fig. 4(a)–(d). Contrary to all expectations, no lithium insertion occurs above 1.7 V (versus lithium).

The composite electrodes $MnV_2O_{6+\delta}$+C exhibit a large capacity during the first discharge down to 10 mV (versus lithium) (Fig. 4(a)–(d)). Within this voltage range, lithium insertion can also occur in the carbon black used to enhance the electronic conductivity of the composite electrode. Therefore, the carbon contribution was withdrawn from the total capacity according to a method described in Ref. [4]. The resulting chronopotentiometric curve, for $MnV_2O_{6.96}$, is displayed in Fig. 5. It shows that the first and second discharge curves exhibit similar shapes suggesting that during the first discharge down to 10 mV, the material undergoes a transfor-

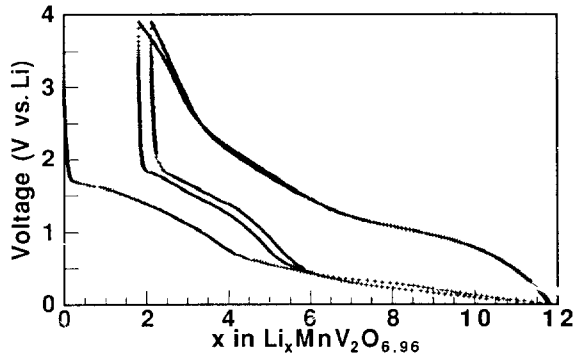

Fig 5. Intrinsic voltage–capacity curve for $MnV_2O_{6.96}$

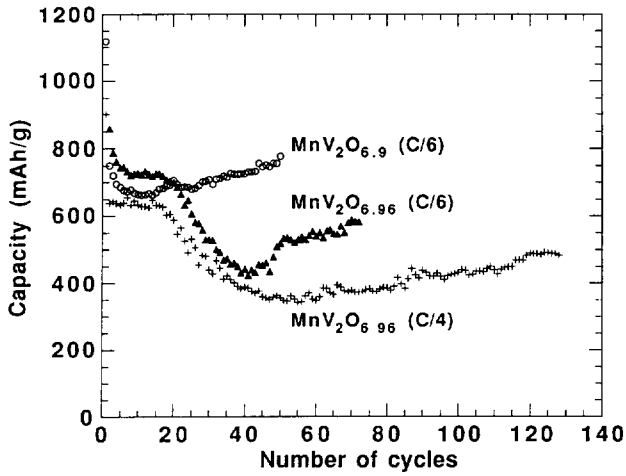

Fig. 6. Cycling behavior of $MnV_2O_{6.90}$ at $C/6$, $MnV_2O_{6.96}$ at $C/4$ and $C/6$ in the 3.9–0.01 V voltage range.

mation which is mostly reversible. The intrinsic reversible capacity of $MnV_2O_{6.96}$ is about 10 Li per formula unit.

Fig. 4(a)–(d) shows that lithium can be inserted reversibly in all $MnV_2O_{6+\delta}$ materials with an irreversible loss of capacity in the course of the first discharge/charge cycle, a loss that increases when δ decreases. In MnV_2O_6 (Fig. 4(e)), a first insertion step occurs at 2.4 V. It corresponds to 2 Li ions per formula unit and is likely to be related to the reduction of V^{5+} to V^{4+}. If the discharge is continued down to 10 mV, a large capacity is observed which, however, is not recovered during the next charge.

The cycling behavior of composite electrodes containing $MnV_2O_{6.90}$ and $MnV_2O_{6.96}$ materials (which exhibit the highest reversible capacities at the first cycle) was tested between 10 mV and 3.9 V in galvanostatic mode over more than 100 discharge/charge cycles at cycling rates of $C/6$ or $C/4$. Fig. 6 shows that the reversible capacity decreases over the first severals tens of cycles and then increases to reach almost stable values after about 100 cycles. This behavior is not clearly understood; it could come from a kind of 'electrochemical grinding' of the material particles, leading to further smaller grains that present a more favorable overall kinetics [5].

5. Characterization of the lithium-inserted derivatives

The very high values reported for the intrinsic reversible capacities of $MnV_2O_{6+\delta}$ materials formally would correspond to an almost complete reduction of the transition metal cations. This point raises important questions concerning structural aspects and electronic transfers to which investigations by local techniques can shed some light.

Therefore, XAS experiments have been undertaken on different $Li_xMnV_2O_{6.96}$ compositions hereafter labelled A, B ··· E. Materials B to E were obtained from A ($MnV_2O_{6.96}$) after the following electrochemical steps:

- half a discharge for B ($\sim Li_6MnV_2O_{6.96}$),
- a complete discharge for C ($\sim Li_{12}MnV_2O_{6.96}$),
- a complete discharge + half a charge for D ($\sim Li_6MnV_2O_{6.96}$),
- a complete discharge/charge cycle for E ($\sim Li_2MnV_2O_{6.96}$).

EELS experiments were done on slightly different compositions reported in Table 3. Average oxidation states of V and Mn were inferred from the position in energy of the l_3 line.

5.1. Evolution of the V oxidation state and of the VO_n polyhedron

The presence of a single V–O peak in the RDFs of compounds B to E indicates that after electrochemical treatment the V–O distances become much closer to each other than they were in the starting material A, for which three V–O peaks are observed. These V–O peaks were refined.

For B and D the V–O distances are 2.02 and 2.03 Å, respectively. It is slightly longer for C, e.g. 2.05 Å. In these three cases the refinement leads to a number of oxygen neighbors close to six. Accordingly, on the XANES spectra of B, C and D, the pre-edge peak intensities are weak (Fig. 7) which indicates that V occupies a rather symmetrical site.

After a complete discharge/charge cycle (compound E) the V–O distance becomes much shorter, e.g. 1.73 Å, and the number of oxygen neighbors is four. Accordingly, the pre-edge peak intensity (XANES spectrum) is very large, even larger than for the starting material A (Fig. 7).

Table 3
Average oxidation states of V and Mn in $Li_xMnV_2O_{6.96}$ compounds (inferred from EELS experiments)

x in $Li_xMnV_2O_{6.96}$	Oxidation state (±0.2) of	
	V	Mn
0	5.0	4.0
7	3.8	2.1
10	3.3	2.0
4 [a]	4.3	2.5
1.5	5.0	2.6

[a] Sample prepared by a complete discharge + partial charge

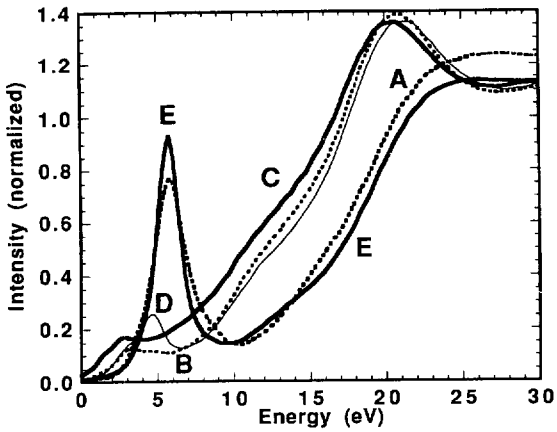

Fig. 7. Normalized V *k*-edge XANES spectra of compounds A to E.

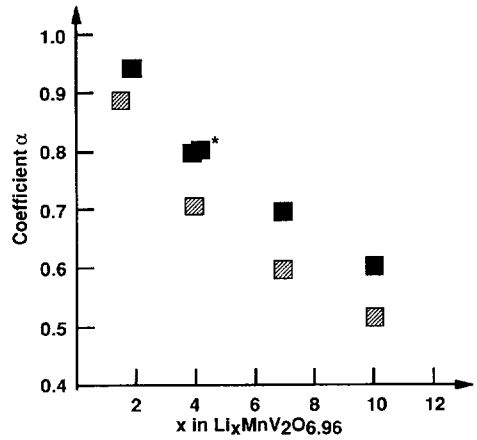

Fig. 9. Evolution of α as a function of x in the $Li_xMnV_2O_{6.96}$ compounds (α from method 1: hatched squares, α from method 2: black squares; * sample prepared by a complete discharge + partial charge)

On account of these results and of average oxidation states given in Table 3 the following evolution can be proposed for V: upon half a discharge (compound B) V, as a mixture of V^{3+} and V^{4+} cations, is in a sixfold rather symmetrical environment of O atoms (likely to be octahedral). A similar environment is observed for compound C (complete discharge) with an average oxidation state close to (+3). During the following charge, V in compound D (half a charge) appears as similar to V in B, and becomes V^{5+} in a tetrahedral coordination after a complete discharge/charge cycle (compound E).

5.2. *Evolution of the Mn oxidation state and of the MnO_n polyhedron*

An important increase of the Mn–O peak width is observed in the RDFs of compounds B to E. This indicates a dispersion of the Mn–O distances likely related with the coexistence of several oxidation states. As a consequence, the refinements were difficult and for compound C they are still in progress. However, it appears that the lithium insertion induces an important increase of the Mn–O distances which do not decrease significantly during the following charge (~2.1 Å in compounds B, D and E). The XANES spectra show that the pre-edge peak intensity remains weak for these three latter compounds, thus indicating that the oxygen polyhedron around Mn likely remains octahedral (Fig. 8). For compound C it was not possible to draw meaningful conclusions from the XAS study. However, EELS results (Table 3) clearly show that Mn^{4+} cations are reduced to Mn^{2+} during the first dicharge. This Mn reduction process is not reversible: at the end of the first discharge/charge cycle the material contains almost equal amounts of Mn^{3+} and Mn^{2+} cations.

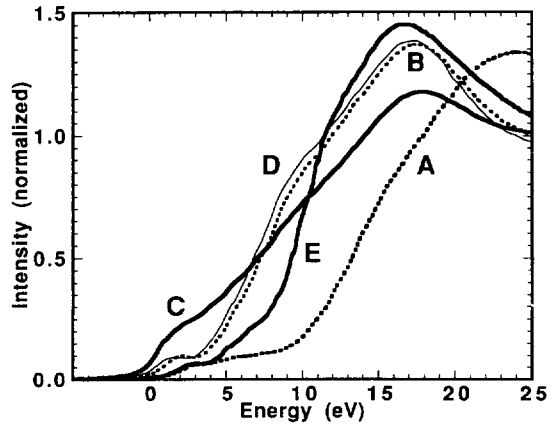

Fig. 8. Normalized Mn *k*-edge XANES spectra of compounds A to E.

5.3. *Investigations of the electronic transfer from lithium to the host matrix*

Let α be a coefficient describing the electronic transfer of lithium to the $Li_xMnV_2O_{6.96}$ host matrix. α was determined using two different methods for various x values:

(i) the first method is based on an electroneutrality equation where the various charges are taken as equal to α for Li, −2 for oxygen while those of the transition metal cations are assimilated to their oxidation states (d_{Mn} and d_V for Mn and V, respectively) inferred from EELS experiments. They were introduced in the following electroneutrality equation:

$$x\alpha + d_{Mn} + 2d_V - (2 \times 6.96) = 0$$

(ii) in the second method α is determined by EELS from a direct measurement of the Li *k*-edge energy, with the use of an arbitrary scale taking α as equal to 0 and 1, respectively, for the energy measured with Li metal and Li_2S.

These two sets of α values appear in Fig. 9 which shows a decrease of the electronic transfer from lithium to the host matrix with increasing x, whichever method was used to determine α. Investigations concerning lithium species and insertion/de-insertion mechanisms in these materials are presently in progress.

References

[1] P. Faber and J. Brenet, *Ger. Patent No. 2 419 490* (1968).
[2] V.L. Zolotavin, V.N. Bulygina and I.Ya. Bezrukov, *Russ. J. Inorg. Chem., 15* (1970) 222.
[3] J.L. Mansot, P. Leone, P. Euzen and P. Palvadeau, *Microsc. Microanal. Microstruct., 5* (1994) 79.
[4] D. Guyomard and J.-M. Tarascon, *J. Electrochem. Soc., 140* (1993) 3071.
[5] J.-M Tarascon, personal communication.